Available online at www.sciencedirect.com
SCIENCE DIRECT®
European Journal of Mechanics B/Fluids 25 (2006) 113–129

Surface effects in rarefied gas dynamics: an analysis based on the Cercignani–Lampis boundary condition

R.F. Knackfuss [a,1], L.B. Barichello [b,*]

[a] *Programa de Pós-Graduação em Engenharia Mecânica, Universidade Federal do Rio Grande do Sul, Rua Sarmento Leite, 425, 90050-170 Porto Alegre, RS, Brazil*
[b] *Instituto de Matemática, Universidade Federal do Rio Grande do Sul, Av. Bento Gonçalves, 9500 – Campus do Vale, 91509-900 Porto Alegre, RS, Brazil*

Received 29 December 2004; received in revised form 14 April 2005; accepted 20 April 2005

Available online 26 May 2005

Abstract

The flow of a rarefied gas, in a plane channel, is investigated, with special attention to the gas–surface interaction, modeled by the Cercignani–Lampis kernel that is defined in terms of normal and tangential accommodation coefficients. An analytical version of the discrete-ordinates method is used to solve, in an unified approach, the Poiseuille flow, thermal-creep flow and Couette flow problems with kinetic equations defined in terms of the BGK model. Numerical results for the velocity and heat-flow profiles and flow rates are reported, for a wide range of the accommodation coefficients and the Knudsen number.
© 2005 Elsevier SAS. All rights reserved.

Keywords: Rarefied gas dynamics; Kinetic equations; Discrete-ordinates method; Cercignani–Lampis kernel

1. Introduction

It is known that, in the analysis of a rarefied gas flow, in microscales, its interaction with surfaces plays a very important role [1]. In particular, the material surface – its type and roughness – determines the gas–wall interaction, which leads to the definition of different accommodation coefficients [2]. In the mathematical modeling of the problem, the boundary conditions take into account the wall type via the scattering kernel. Different types of scattering kernels express different gas–surface interactions, as for example, the well known Maxwell's scattering kernel [3], where it is considered that some fraction $1-\alpha$ of the particles is reflected specularly and the remaining fraction α is reflected diffusely.

Other kernels have been proposed and studied over the years [4,5]. In this sense, the idea of looking for better physical representation of the surfaces, mainly considering more than one accommodation coefficient, has been pursued. In this context, the Cercignani–Lampis model [6], which introduces two accommodation coefficients – the tangential accommodation coefficient ($\alpha_t \in [0, 2]$) and the normal accommodation coefficient ($\alpha_n \in [0, 1]$) – is very well known. In recent works [7–9] a numerical methodology (the discrete-velocities method) was used to solve, based on the S-model kinetic equations, some classical problems of the rarefied gas dynamics, including the Cercignani–Lampis kernel. A numerical technique [10] applied to the integral

* Corresponding author.
E-mail addresses: rfk.sma@terra.com.br (R.F. Knackfuss), lbaric@mat.ufrgs.br (L.B. Barichello).
[1] Permanent Address: Departamento de Matemática, Universidade Federal de Santa Maria, RS, Brasil.

0997-7546/$ – see front matter © 2005 Elsevier SAS. All rights reserved.
doi:10.1016/j.euromechflu.2005.04.003

form of the Boltzmann equation, was also used for the solution of the Poiseuille flow problem, with this type of boundary conditions.

In particular, this kernel has also been associated to the modeling of some problems which have been solved by a recent analytical version of the discrete-ordinates method, the ADO method [11]. In fact, in a series of recent works [12–19], the ADO method has been used to provide "unified" solutions for a class of problems based on kinetic equations (the BGK model [20], the S model [21], the CLF model [22,23], the CES model [24]) and the linearized Boltzmann equation [25].

In trying to obtain a wide class of problems solved by the same methodology, which has analytical character, adequate to deal with different problems and different model equations, the use of the Cercignani–Lampis boundary conditions along with the ADO method, has been also investigated. In this way, results for the Poiseuille flow and thermal-creep flow, based on the BGK model and the S-model equations [26–28] were obtained as well as results for the slip coefficients, based on the BGK model, the S-model and the linearized Boltzmann equation [27,29].

In this work, keeping in mind the development of this analysis, based on the use of the Cercignani–Lampis boundary conditions associated with the ADO method, and the interest of providing results for surface effects study which is so important in microscales phenomena, we consider, in an unified approach, the solution of the Poiseuille flow problem, the thermal creep flow problem and the Couette problem, based on the BGK model equation and the Cercignani–Lampis kernel for describing the gas–surface interaction.

2. General formulation

We consider, as a starting point of this work, the kinetic equation written in terms of a perturbation $h(y, \mathbf{c})$, to the distribution function from a local Maxwellian, as [3,24]

$$c_y \frac{\partial}{\partial y} h(y, \mathbf{c}) + \varepsilon h(y, \mathbf{c}) = \varepsilon \pi^{-3/2} \int_{-\infty}^{\infty} \int_{-\infty}^{\infty} \int_{-\infty}^{\infty} \mathrm{e}^{-c'^2} h(y, \mathbf{c}') F(\mathbf{c}' : \mathbf{c}) \, \mathrm{d}c'_x \, \mathrm{d}c'_y \, \mathrm{d}c'_z + S(\mathbf{c}), \tag{1}$$

where we follow [26] and we write the kernel $F(\mathbf{c}' : \mathbf{c})$ as

$$F(\mathbf{c}' : \mathbf{c}) = 1 + 2(\mathbf{c}' \cdot \mathbf{c}) + \frac{2}{3}\left(c'^2 - \frac{3}{2}\right)\left(c^2 - \frac{3}{2}\right) + \beta M(\mathbf{c}' : \mathbf{c}), \tag{2}$$

with

$$M(\mathbf{c}' : \mathbf{c}) = \frac{4}{15}(\mathbf{c}' \cdot \mathbf{c})\left(c'^2 - \frac{5}{2}\right)\left(c^2 - \frac{5}{2}\right), \tag{3}$$

and where the case $\beta = 0$ defines the well known BGK model equation [20] that will be the basis for establishing the numerical results, in this work. We note that we chose here to write the expression for the kernel, as in Eq. (2), because it includes also the case $\beta = 1$ that defines the S-model [21], another constant collision frequency model, in terms of which some numerical comparisons will be established, later on in this work.

In regard to Eq. (1), we use the dimensionless (written in terms of a mean-free path l) spatial variable y, the three components of the velocity vector (c_x, c_y, c_z) are expressed in dimensionless units and

$$\varepsilon = \sigma_0^2 n_0 \pi^{1/2} l, \tag{4}$$

where σ_0 is the collision diameter of the gas particles (in the rigid-sphere approximation) and n_0 is the (constant) density of gas particles. Continuing, considering the problems we want to investigate in this work, we write

$$S(\mathbf{c}) = -c_x\left[k_1 + k_2(c_x^2 + c_y^2 + c_z^2 - 5/2) + 2k_3 c_y\right], \tag{5}$$

where the choices ($k_1 \neq 0$, arbitrary and $k_2 = k_3 = 0$), ($k_1 = k_3 = 0$ and $k_2 \neq 0$, arbitrary) define, respectively, the Poiseuille flow and the thermal-creep flow problems. In fact, k_1 and k_2 are the constant gradients (in dimensionless units) of the density and temperature [3]. Still, the choice ($k_1 = k_2 = 0$ and $k_3 \neq 0$, arbitrary) is associated, here, with the Couette flow problem. In this last case, we consider that k_3 is the gradient of the (linear) velocity [3] which, at the boundary, we define to be equal to the velocity of the wall u_w.

For plane channel problems, $y \in [-a, a]$, we supplement Eq. (1) with boundary conditions. In this work, we use the Cercignani–Lampis boundary conditions [6,26] such that

$$h(-a, c_x, c_y, c_z) = \int_0^{\infty} \int_{-\infty}^{\infty} \int_{-\infty}^{\infty} h(-a, c'_x, -c'_y, c'_z) R(c'_x, -c'_y, c'_z : c_x, c_y, c_z) \, \mathrm{d}c'_x \, \mathrm{d}c'_z \, \mathrm{d}c'_y \tag{6a}$$

and

$$h(a, c_x, -c_y, c_z) = \int_0^{\infty}\int_{-\infty}^{\infty}\int_{-\infty}^{\infty} h(a, c'_x, c'_y, c'_z) R(c'_x, c'_y, c'_z : c_x, -c_y, c_z)\, \mathrm{d}c'_x\, \mathrm{d}c'_z\, \mathrm{d}c'_y. \tag{6b}$$

Here

$$R(c'_x, c'_y, c'_z : c_x, c_y, c_z) = \frac{2c'_y}{\pi\alpha_n\alpha_t(2-\alpha_t)} T(c'_x : c_x) S(c'_y : c_y) T(c'_z : c_z) \tag{7}$$

with

$$T(x : z) = \exp\left[-\frac{[(1-\alpha_t)z - x]^2}{\alpha_t(2-\alpha_t)}\right] \tag{8}$$

and

$$S(x : z) = \exp\left[-\frac{[(1-\alpha_n)^{1/2}z - x]^2}{\alpha_n}\right] \hat{I}_0\left[\frac{2(1-\alpha_n)^{1/2}|xz|}{\alpha_n}\right]. \tag{9}$$

For computational purposes, we write

$$\hat{I}_0(w) = I_0(w)\, \mathrm{e}^{-w} \tag{10}$$

where $I_0(w)$ is the modified Bessel function,

$$I_0(w) = \frac{1}{2\pi}\int_0^{2\pi} \mathrm{e}^{w\cos\phi}\, \mathrm{d}\phi. \tag{11}$$

As we see in Eqs. (7) to (9), the Cercignani–Lampis kernel [25] is defined in terms of two accommodation coefficients [21,29]: $\alpha_t \in [0, 2]$ the accommodation coefficient of tangential momentum and $\alpha_n \in [0, 1]$ the accommodation coefficient of energy corresponding to the normal component of velocity. According to the literature [7] the use of these two accommodation coefficient allows a better physical representation of the roughness effects.

The quantities of interest, we seek to compute in this work, as for example [26], the velocity profile

$$u(y) = \pi^{-3/2} \int_{-\infty}^{\infty}\int_{-\infty}^{\infty}\int_{-\infty}^{\infty} \mathrm{e}^{-c^2} h(y, c_x, c_y, c_z) c_x\, \mathrm{d}c_x\, \mathrm{d}c_y\, \mathrm{d}c_z, \tag{12}$$

the heat-flow profile

$$q(y) = \pi^{-3/2} \int_{-\infty}^{\infty}\int_{-\infty}^{\infty}\int_{-\infty}^{\infty} \mathrm{e}^{-c^2} h(y, c_x, c_y, c_z)\left(c^2 - \frac{5}{2}\right) c_x\, \mathrm{d}c_x\, \mathrm{d}c_y\, \mathrm{d}c_z, \tag{13}$$

and, for the Couette flow problem, a component of the pressure tensor

$$P_{xy} = \pi^{-3/2} \int_{-\infty}^{\infty}\int_{-\infty}^{\infty}\int_{-\infty}^{\infty} \mathrm{e}^{-c^2} h(y, c_x, c_y, c_z) c_x c_y\, \mathrm{d}c_x\, \mathrm{d}c_y\, \mathrm{d}c_z, \tag{14}$$

are defined in terms of some moments, or integrals, of the h function. Next in this work, we use this fact to develop simpler problems, derived from Eq. (1), which will be solved with the discrete ordinates approach – the ADO method [11].

Before proceeding to the development of the discrete ordinates solution that will be used to evaluate Eqs. (12), (13) and (14), we note that, since we will be working with the BGK model, in this work, from this point, we use $\varepsilon = 1$ in Eq. (1). In fact, this is the resulting numerical value [24], for the BGK model, when a mean-free path based on either viscosity or conductivity is used to evaluate Eq. (4).

3. A vector formulation

In order to get simpler formulations to evaluate the quantities of interest, we start by multiplying Eq. (1) by

$$\phi_1(c_x, c_z) = (c_x/\pi)\, \mathrm{e}^{-(c_x^2 + c_z^2)} \tag{15}$$

and we integrate over all c_x and c_z, such that, if we introduce the new notation $\xi = c_y$, and we define

$$h_1(y,\xi) = \int_{-\infty}^{\infty}\int_{-\infty}^{\infty} \phi_1(c_x,c_z)h(y,c_x,\xi,c_z)\,\mathrm{d}c_x\,\mathrm{d}c_z \tag{16}$$

we find that

$$\xi\frac{\partial}{\partial y}h_1(y,\xi) + h_1(y,\xi) = \pi^{-1/2}\int_{-\infty}^{\infty} \mathrm{e}^{-\xi'^2}h_1(y,\xi')\,\mathrm{d}\xi' + a_1(\xi) \tag{17}$$

where

$$a_1(\xi) = \int_{-\infty}^{\infty}\int_{-\infty}^{\infty} \phi_1(c_x,c_z)S(c_x,\xi,c_z)\,\mathrm{d}c_x\,\mathrm{d}c_z. \tag{18}$$

As a second step, we multiply Eq. (1) by

$$\phi_2(c_x,c_z) = \frac{2^{-1/2}}{\pi}c_x(c_x^2+c_z^2-2)\,\mathrm{e}^{-(c_x^2+c_z^2)} \tag{19}$$

such that, if we define,

$$h_2(y,\xi) = \int_{-\infty}^{\infty}\int_{-\infty}^{\infty} \phi_2(c_x,c_z)h(y,c_x,\xi,c_z)\,\mathrm{d}c_x\,\mathrm{d}c_z \tag{20}$$

and follow analogous procedure to the one described above, we find

$$\xi\frac{\partial}{\partial y}h_2(y,\xi) + h_2(y,\xi) = a_2(\xi) \tag{21}$$

with

$$a_2(\xi) = \int_{-\infty}^{\infty}\int_{-\infty}^{\infty} \phi_2(c_x,c_z)S(c_x,\xi,c_z)\,\mathrm{d}c_x\,\mathrm{d}c_z. \tag{22}$$

To be more specific, considering the Poiseuille flow, thermal-creep flow and Couette flow problems, that we discuss in this work, in Eq. (18),

$$a_1(\xi) = -\frac{k_1}{2} + \frac{k_2}{2}\left(\frac{1}{2}-\xi^2\right) - k_3\xi \tag{23}$$

and, in Eq. (22),

$$a_2(\xi) = \sqrt{2}\left(-\frac{k_2}{2}\right). \tag{24}$$

In this way, we let $\mathbf{H}(y,\xi)$, to be the vector with components $h_1(y,\xi)$ and $h_2(y,\xi)$ and we rewrite Eqs. (17) to (24) in a more appropriate matrix form as

$$\xi\frac{\partial}{\partial y}\mathbf{H}(y,\xi) + \mathbf{H}(y,\xi) = \int_{-\infty}^{\infty} \boldsymbol{\Psi}(\xi')\mathbf{H}(y,\xi')\,\mathrm{d}\xi' + \mathbf{S}^*(\xi), \tag{25}$$

where

$$\boldsymbol{\Psi}(\xi') = \pi^{-1/2}\,\mathrm{e}^{-\xi'^2}\mathbf{Q} \tag{26}$$

with

$$\mathbf{Q} = \begin{bmatrix} 1 & 0 \\ 0 & 0 \end{bmatrix}. \tag{27}$$

In Eq. (25), the components of the vector $\mathbf{S}^*(\xi)$ are defined by $a_1(\xi)$ and $a_2(\xi)$ given, respectively, by Eqs. (23) and (24). We recall that for defining the Poiseuille flow problem we use $k_1 \neq 0$, $k_2 = k_3 = 0$, in the expressions above; for the thermal-creep problem we use $k_1 = k_3 = 0$ and $k_2 \neq 0$, while, for the Couette flow problem we use $k_1 = k_2 = 0$ and $k_3 \neq 0$.

The proposed procedure, derived from Eqs. (15) and (19), is also applied to the boundary conditions. We find, from Eqs. (6), that

$$\mathbf{H}(-a,\xi) = \mathbf{A}\int_0^\infty \mathbf{H}(-a,-\xi')\,f(\xi',\xi)\,\mathrm{d}\xi' \tag{28a}$$

and

$$\mathbf{H}(a,-\xi) = \mathbf{A}\int_0^\infty \mathbf{H}(a,\xi')\,f(\xi',\xi)\,\mathrm{d}\xi' \tag{28b}$$

with

$$\mathbf{A} = \begin{bmatrix} 1-\alpha_t & 0 \\ 0 & (1-\alpha_t)^3 \end{bmatrix} \tag{29}$$

and

$$f(\xi',\xi) = \frac{2\xi'}{\alpha_n}\,\exp\left[-\frac{[(1-\alpha_n)^{1/2}\xi - \xi']^2}{\alpha_n}\right]\hat{I}_0\left[\frac{2(1-\alpha_n)^{1/2}\xi'\xi}{\alpha_n}\right]. \tag{30}$$

We can also express the quantities of interest, defined in Eqs. (12) to (14), in terms of the vector notation, as

$$u(y) = \pi^{-1/2}\int_{-\infty}^{\infty} \mathrm{e}^{-\xi^2}[1 \quad 0]\mathbf{H}(y,\xi)\,\mathrm{d}\xi, \tag{31}$$

$$q(y) = \pi^{-1/2}\int_{-\infty}^{\infty} \mathrm{e}^{-\xi^2}\left[(\xi^2 - 1/2) \quad \sqrt{2}\right]\mathbf{H}(y,\xi)\,\mathrm{d}\xi \tag{32}$$

and

$$P_{xy} = \pi^{-1/2}\int_{-\infty}^{\infty} \mathrm{e}^{-\xi^2}[1 \quad 0]\mathbf{H}(y,\xi)\xi\,\mathrm{d}\xi. \tag{33}$$

We now proceed to develop a discrete-ordinates solution for the problem given by Eq. (25) with boundary conditions given by Eqs. (28). In fact, as we will see later on in this text, we can also consider for these problems we solve in this work, in regard to the boundary conditions, Eq. (28b), for example, along with either a symmetry condition

$$\mathbf{H}(y,\xi) = \mathbf{H}(-y,-\xi) \tag{34}$$

or an anti-symmetry condition

$$\mathbf{H}(-y,-\xi) = -\mathbf{H}(y,\xi) \tag{35}$$

to specify the behavior at the boundaries.

Finally, looking back to Eqs. (17), (21), (23) and (24), and noting the homogeneous boundary conditions, it is easy to see that, for the Poiseuille flow problem ($k_1 \neq 0$ and $k_2 = k_3 = 0$) one may choose to deal only with the h_1 problem. In fact, this approach was already used by Knackfuss and Barichello [28] along with a variation of the ADO method based on explicit expressions for the elementary solutions independent of the spatial variable. On the other hand, Eq. (21) could also be solved, in principle, analytically. In this work, however, we chose to work in the vector formulation derived above, to develop a procedure which could be, as much as possible, "unified" for dealing with all the three problems at the same time and also because a similar vector formulation has been used for solving problems based on other model equations, by the ADO method [13–15,17].

4. The development

First of all, we note the source term in Eq. (25) and write

$$\mathbf{H}(y,\xi) = \mathbf{H}^h(y,\xi) + \mathbf{H}^p(y,\xi). \tag{36}$$

Keeping in mind the specific definition of the source term, depending on the choices of k_1, k_2 and k_3, we then seek for particular solutions of a form

$$\mathbf{H}^p(y,\xi) = \mathbf{B}y^2 + \mathbf{C}y\xi + \mathbf{D}\xi^2 + \mathbf{E}\xi + \mathbf{F}, \tag{37}$$

where **B**, **C**, **D**, **E** and **F** are constant vectors, and we find

$$\mathbf{H}^p(y,\xi) = \frac{1}{2}\begin{bmatrix} k_1(y^2 - 2y\xi + 2\xi^2) + k_2(1/2 - \xi^2) - k_3\xi \\ -k_2\sqrt{2} \end{bmatrix}, \tag{38}$$

such that, if we substitute Eq. (36) in Eqs. (25) and (28b) we obtain that the homogeneous solution satisfies the problem

$$\xi\frac{\partial}{\partial y}\mathbf{H}^h(y,\xi) + \mathbf{H}^h(y,\xi) = \int_{-\infty}^{\infty} \boldsymbol{\Psi}(\xi')\mathbf{H}^h(y,\xi')\,\mathrm{d}\xi' \tag{39}$$

with $\boldsymbol{\Psi}(\xi)$ given by Eq. (26) and the boundary condition

$$\mathbf{H}^h(a,-\xi) - \mathbf{A}\int_0^{\infty} \mathbf{H}^h(a,\xi')f(\xi',\xi)\,\mathrm{d}\xi' = \mathbf{R}(\xi). \tag{40}$$

For the Poiseuille flow and thermal-creep flow problem, along with Eq. (40) we consider the symmetry condition given by Eq. (34); for the Couette flow problem, Eq. (35), the anti-symmetry condition is considered. Still, here, $f(\xi',\xi)$ is defined in Eq. (30),

$$\mathbf{A} = \begin{bmatrix} 1-\alpha_t & 0 \\ 0 & (1-\alpha_t)^3 \end{bmatrix} \tag{41}$$

and

$$\mathbf{R}(\xi) = \mathbf{A}\int_0^{\infty} \mathbf{H}^p(a,\xi')f(\xi',\xi)\,\mathrm{d}\xi' - \mathbf{H}^p(a,-\xi). \tag{42}$$

4.1. A discrete-ordinates solution

We solve the homogeneous problem, defined by Eqs. (39) to (42), with the ADO approach [11]. Thus, we define a N points "half-range" quadrature scheme and we write the discrete-ordinates version of Eq. (39) in the form

$$\pm\xi_i\frac{d}{dy}\mathbf{H}^h(y,\pm\xi_i) + \mathbf{H}^h(y,\pm\xi_i) = \sum_{k=1}^{N}\omega_k\boldsymbol{\Psi}(\xi_k)\big[\mathbf{H}^h(y,\xi_k) + \mathbf{H}^h(y,-\xi_k)\big], \tag{43}$$

for $i = 1, 2, \ldots, N$, where we emphasize that the N nodes and weights $\{\xi_k, \omega_k\}$ are defined for evaluating integrals over the interval $[0,\infty)$.

We seek for solutions of Eqs. (43) of the exponential form

$$\mathbf{H}^h(y,\xi) = \boldsymbol{\Phi}(\nu,\xi)\,\mathrm{e}^{-y/\nu} \tag{44}$$

to obtain

$$(\nu \mp \xi_i)\boldsymbol{\Phi}(\nu,\pm\xi_i) = \nu\sum_{k=1}^{N}\omega_k\boldsymbol{\Psi}(\xi_k)\big[\boldsymbol{\Phi}(\nu,\xi_k) + \boldsymbol{\Phi}(\nu,-\xi_k)\big]. \tag{45}$$

We then let $\boldsymbol{\Phi}_+(\nu)$ and $\boldsymbol{\Phi}_-(\nu)$ be $2N\times 1$ vectors, the each 2×1 components of which are, respectively, $\boldsymbol{\Phi}(\nu,\xi_k)$ and $\boldsymbol{\Phi}(\nu,-\xi_k)$, such that, in writing

$$\mathbf{U} = \boldsymbol{\Phi}_+(\nu) + \boldsymbol{\Phi}_-(\nu) \tag{46}$$

we obtain, after some manipulations [11], from Eq. (44) evaluated at $\xi = \pm\xi_k$, an eigenvalue problem

$$(\mathbf{D} - 2\mathbf{W})\mathbf{U} = \lambda\mathbf{U}. \tag{47}$$

Here

$$\lambda = 1/\nu^2, \tag{48}$$

$$\mathbf{D} = \operatorname{diag}\left\{\left(\frac{1}{\xi_1}\right)^2\mathbf{I}, \left(\frac{1}{\xi_2}\right)^2\mathbf{I}, \ldots, \left(\frac{1}{\xi_N}\right)^2\mathbf{I}\right\}, \tag{49}$$

with $\mathbf{I}$ denoting the 2×2 identity matrix and $\mathbf{W}$ the $2N \times 2N$ matrix where each $2 \times 2N$ submatrix is defined as

$$\mathbf{R}_i = \left(\frac{1}{\xi_i}\right)^2\big[\omega_1\boldsymbol{\Psi}(\xi_1) \quad \omega_2\boldsymbol{\Psi}(\xi_2) \quad \ldots \quad \omega_N\boldsymbol{\Psi}(\xi_N)\big], \tag{50}$$

for $i = 1, 2, \ldots, N$. We also recall here Eq. (26).

From Eq. (47) we obtain a set of eigenvalues and eigenvectors $\{\lambda_j, \mathbf{U}_j\}$, for $j = 1, 2, \ldots, 2N$ in terms of which we find we can write

$$\boldsymbol{\Phi}_+(\nu_j) = \frac{1}{2\nu_j}\operatorname{diag}\big\{(\nu_j + \xi_1)\mathbf{I}, (\nu_j + \xi_2)\mathbf{I}, \ldots, (\nu_j + \xi_N)\mathbf{I}\big\}\mathbf{U}_j \tag{51a}$$

and

$$\boldsymbol{\Phi}_-(\nu_j) = \frac{1}{2\nu_j}\operatorname{diag}\big\{(\nu_j - \xi_1)\mathbf{I}, (\nu_j - \xi_2)\mathbf{I}, \ldots, (\nu_j - \xi_N)\mathbf{I}\big\}\mathbf{U}_j, \tag{51b}$$

where ν_j is the positive square root of $1/\lambda_j$ and now $\mathbf{I}$ is the 2×2 identity matrix. At this point, we write

$$\mathbf{H}^h_\pm(y) = \sum_{j=1}^{2N}\big[A_j\boldsymbol{\Phi}_\pm(\nu_j)\,\mathrm{e}^{-(a+y)/\nu_j} + B_j\boldsymbol{\Phi}_\mp(\nu_j)\,\mathrm{e}^{-(a-y)/\nu_j}\big]. \tag{52}$$

As usual, for conservative problems [12] it is expected that (at least) one of the separation constants, ν_1 for example, becomes unbounded as N tends to infinity. Thus, in this work, we write the final form of the solution for the homogeneous problem as

$$\mathbf{H}^h_\pm(y) = A_1\boldsymbol{\Phi}^1 + B_1\boldsymbol{\Phi}^2_\pm(y) + \sum_{j=2}^{2N}\big[A_j\boldsymbol{\Phi}_\pm(\nu_j)\,\mathrm{e}^{-(a+y)/\nu_j} + B_j\boldsymbol{\Phi}_\mp(\nu_j)\,\mathrm{e}^{-(a-y)/\nu_j}\big], \tag{53}$$

where the $2N \times 1$ exact solutions, $\boldsymbol{\Phi}^1$, defined by N (vector) components of the form

$$\mathbf{F}^1 = \begin{bmatrix} 1 \\ 0 \end{bmatrix} \tag{54}$$

and $\boldsymbol{\Phi}^2_\pm(y)$, with N (vector) components

$$\mathbf{F}^2_\pm(y) = \begin{bmatrix} y \mp \xi \\ 0 \end{bmatrix}, \tag{55}$$

were introduced.

Still, to establish the final solution for the homogeneous problem, for the Poiseuille flow and thermal-creep flow problems, we first consider the symmetry condition and rewrite the general solution, Eq. (53), as

$$\mathbf{H}^h_\pm(y) = A_1\boldsymbol{\Phi}^1 + \sum_{j=2}^{2N}A_j\big[\boldsymbol{\Phi}_\pm(\nu_j)\,\mathrm{e}^{-(a+y)/\nu_j} + \boldsymbol{\Phi}_\mp(\nu_j)\,\mathrm{e}^{-(a-y)/\nu_j}\big] \tag{56}$$

and we then obtain the arbitrary constants A_j, for $j = 1, \ldots, N$ by evaluating the boundary condition given in Eq. (40) at the quadrature points. In other words, we solve the linear algebraic system, for $i = 1, \ldots, N$,

$$A_1\left\{\boldsymbol{\Phi}^1 - \left[\mathbf{A}^*\boldsymbol{\Phi}^1\sum_{k=1}^{N}\omega_k f(\xi_k, \xi_i)\right]\right\} + \sum_{j=2}^{2N}A_j\left\{\big[\boldsymbol{\Phi}_-(\nu_j)\,\mathrm{e}^{-2a/\nu_j} + \boldsymbol{\Phi}_+(\nu_j)\big]\right.$$
$$\left. - \left[\sum_{k=1}^{N}\omega_k f(\xi_k, \xi_i)\mathbf{A}^*\big[\boldsymbol{\Phi}_+(\nu_j)\,\mathrm{e}^{-2a/\nu_j} + \boldsymbol{\Phi}_-(\nu_j)\big]\right]\right\} = \mathbf{R}^*(\xi_i), \tag{57}$$

where, for $\mathbf{A}$ given in Eq. (41), we define a $2N \times 2N$ matrix

$$\mathbf{A}^* = \operatorname{diag}\{\mathbf{A}, \mathbf{A}, \ldots, \mathbf{A}\}, \tag{58}$$

and each two lines of the $2N \times 1$ vector $\mathbf{R}^*(\xi_i)$ is of the type

$$\mathbf{R}(\xi_i) = \mathbf{A}\sum_{k=1}^{N}\left[\omega_k\ f(\xi_k,\xi)\mathbf{H}^p(a,\xi_k)\right] - \mathbf{H}^p(a,-\xi_i). \tag{59}$$

Once we have established the solution of the homogeneous problem we will define the quantities of interest, for the Poiseuille and thermal-creep flow problems, in terms of the general discrete-ordinates solution of the vector problem as

$$\mathbf{H}_{\pm}(y) = \mathbf{H}^p_{\pm}(y) + A_1\boldsymbol{\Phi}^1 + \sum_{j=2}^{2N} A_j\left[\boldsymbol{\Phi}_{\mp}(\nu_j)\,\mathrm{e}^{-(a+y)/\nu_j} + \boldsymbol{\Phi}_{\pm}(\nu_j)\,\mathrm{e}^{-(a-y)/\nu_j}\right]. \tag{60}$$

Here we let $\mathbf{H}^p_{\pm}(y)$ denotes the $2N\times 1$ vector, the 2×1 components of which are, respectively, $\mathbf{H}^p(y,\pm\xi_k)$.

On the other hand, for the Couette flow problem, in Eq. (53), we consider the anti-symmetry condition, such that we write the solution for the homogeneous problems as

$$\mathbf{H}^h_{\pm}(y) = B_1\boldsymbol{\Phi}^2_{\pm}(y) + \sum_{j=2}^{2N}\left[A_j\boldsymbol{\Phi}_{\pm}(\nu_j)\,\mathrm{e}^{-(a+y)/\nu_j} - \boldsymbol{\Phi}_{\mp}(\nu_j)\,\mathrm{e}^{-(a-y)/\nu_j}\right] \tag{61}$$

and, in this way, the associated linear algebraic system to be solved in order to determine the arbitrary constants is given by

$$B_1\left\{\boldsymbol{\Phi}^2_{-}(y) - \left[\mathbf{A}^*\sum_{k=1}^{N}\omega_k f(\xi_k,\xi_i)\boldsymbol{\Phi}^2_{+}(y)\right]\right\} + \sum_{j=2}^{2N}A_j\left\{\left[\boldsymbol{\Phi}_{-}(\nu_j)\,\mathrm{e}^{-2a/\nu_j} - \boldsymbol{\Phi}_{+}(\nu_j)\right]\right.$$
$$\left. - \left[\sum_{k=1}^{N}\omega_k f(\xi_k,\xi_i)\mathbf{A}^*\left[\boldsymbol{\Phi}_{+}(\nu_j)\,\mathrm{e}^{-2a/\nu_j} - \boldsymbol{\Phi}_{-}(\nu_j)\right]\right]\right\} = \mathbf{R}^*(\xi_i), \tag{62}$$

where $\mathbf{A}^*$ and $\mathbf{R}^*(\xi_i)$ are defined as in Eqs. (58) and (59). Thus, similarly to Eq. (60), for the Couette flow problem, we will evaluate the quantities of interest by using the expression

$$\mathbf{H}_{\pm}(y) = \mathbf{H}^p_{\pm}(y) + B_1\boldsymbol{\Phi}^2_{\pm}(y) + \sum_{j=2}^{2N}\left[A_j\boldsymbol{\Phi}_{\pm}(\nu_j)\,\mathrm{e}^{-(a+y)/\nu_j} - \boldsymbol{\Phi}_{\mp}(\nu_j)\,\mathrm{e}^{-(a-y)/\nu_j}\right]. \tag{63}$$

5. Quantities of interest

In addition to the velocity and heat-flow profiles, Eqs. (31) and (32), we consider in this section, the particle and heat-flow rates, given, respectively by

$$U = \frac{1}{2a^2}\int_{-a}^{a} u(y)\,\mathrm{d}y \tag{64}$$

and

$$Q = \frac{1}{2a^2}\int_{-a}^{a} q(y)\,\mathrm{d}y, \tag{65}$$

for a $(2a)$ channel. We evaluate the discrete-ordinates version of Eqs. (31) to (33), (64) and (65), noting specific definitions for each one of the problems.

In what follows we use the definition of the vector

$$\mathbf{N}(\nu_j) = \left[\omega_1\boldsymbol{\Lambda}(\xi_1)\quad \omega_2\boldsymbol{\Lambda}(\xi_2)\quad \ldots\quad \omega_N\boldsymbol{\Lambda}(\xi_N)\right]\left[\boldsymbol{\Phi}_{+}(\nu_j) + \boldsymbol{\Phi}_{-}(\nu_j)\right], \tag{66}$$

with components $N_1(\nu_j)$ and $N_2(\nu_j)$, where

$$\boldsymbol{\Lambda}(\xi) = \pi^{-1/2}\,\mathrm{e}^{-\xi^2}\begin{bmatrix}1 & 0\\ \xi^2 - 1/2 & \sqrt{2}\end{bmatrix}, \tag{67}$$

and the expressions

$$M_j(y) = A_j\left[\mathrm{e}^{-(a+y)/\nu_j} + \mathrm{e}^{-(a-y)/\nu_j}\right], \tag{68}$$

$$Q_j(y) = A_j\nu_j\left(1 - \mathrm{e}^{-2a/\nu_j}\right), \tag{69}$$

to write:

Poiseuille flow. Velocity and heat-flow profiles

$$u_p(y) = \frac{k_1}{2}(y^2+1) + A_1 + \sum_{j=2}^{2N} M_j(y) N_1(\nu_j), \tag{70}$$

$$q_p(y) = \frac{k_1}{2} + \sum_{j=2}^{2N} M_j(y) N_2(\nu_j); \tag{71}$$

Particle and heat-flow rates

$$U_p = \frac{1}{2a^2}\left[ak_1\left(\frac{a^2}{3}+1\right) + 2aA_1 + 2\sum_{j=2}^{2N} Q_j(y) N_1(\nu_j)\right], \tag{72}$$

$$Q_p = \frac{1}{2a^2}\left[ak_1 + 2\sum_{j=2}^{2N} Q_j(y) N_2(\nu_j)\right]. \tag{73}$$

Thermal-creep flow. Velocity and heat-flow profiles

$$u_t(y) = A_1 + \sum_{j=2}^{2N} M_j(y) N_1(\nu_j), \tag{74}$$

$$q_t(y) = -\frac{5}{4}k_2 + \sum_{j=2}^{2N} M_j(y) N_2(\nu_j); \tag{75}$$

Particle and heat-flow rates

$$U_t = \frac{1}{2a^2}\left[2aA_1 + 2\sum_{j=2}^{2N} Q_j(y) N_1(\nu_j)\right], \tag{76}$$

$$Q_t = \frac{1}{2a^2}\left[-\frac{5}{2}k_2 a + 2\sum_{j=2}^{2N} Q_j(y) N_2(\nu_j)\right]. \tag{77}$$

Couette flow. Velocity and heat-flow profiles

$$u_c(y) = (k_3 + B_1)y + \sum_{j=2}^{2N} A_j\left[\mathrm{e}^{-(a+y)/\nu_j} - \mathrm{e}^{-(a-y)/\nu_j}\right] N_1(\nu_j), \tag{78}$$

$$q_c(y) = \sum_{j=2}^{2N} A_j\left[\mathrm{e}^{-(a+y)/\nu_j} - \mathrm{e}^{-(a-y)/\nu_j}\right] N_2(\nu_j); \tag{79}$$

Particle and heat-flow rates

$$U_c = \frac{1}{2a^2}\left[(k_3 + B_1)\frac{a^2}{2} - \sum_{j=2}^{2N} A_j \nu_j \left(\mathrm{e}^{-a/\nu_j} - 1\right)^2 N_1(\nu_j)\right], \tag{80}$$

$$Q_c = -\frac{1}{2a^2}\left[\sum_{j=2}^{2N} A_j \nu_j \left(\mathrm{e}^{-a/\nu_j} - 1\right)^2 N_2(\nu_j)\right]; \tag{81}$$

Component of the stress tensor

$$P_{xy} = -\left(\frac{k_3}{2} + \frac{B_1}{2}\right). \tag{82}$$

Table 1
Poiseuille flow: velocity profile $u_p(y)$, $2a = 1$, $\alpha_t = 0.5$

y/a	S-CL [26] $\alpha_n = 0.5$	S-CL ($\varepsilon = \varepsilon_t$) $\alpha_n = 0.5$	S-DE [26] $\alpha = \alpha_t$	BGK-CL $\alpha_n = 0.5$	BGK-CL $\alpha_n = 0.01$	BGK-DE [17] $\alpha = \alpha_t$
0.0	–1.77759	–1.78245	–1.79254	–1.76674	–1.77900	–1.77883
0.1	–1.77490	–1.77922	–1.78999	–1.76410	–1.77649	–1.77631
0.2	–1.76680	–1.76949	–1.78228	–1.75614	–1.76889	–1.76873
0.3	–1.75314	–1.75310	–1.76930	–1.74272	–1.75609	–1.75506
0.4	–1.73368	–1.72978	–1.75081	–1.72359	–1.73786	–1.73776
0.5	–1.70799	–1.69908	–1.72642	–1.69834	–1.71382	–1.71376
0.6	–1.67544	–1.66028	–1.69555	–1.66633	–1.68337	–1.68335
0.7	–1.63494	–1.61219	–1.65717	–1.62648	–1.64551	–1.64554
0.8	–1.58454	–1.55263	–1.60946	–1.57685	–1.59845	–1.59850
0.9	–1.51992	–1.47666	–1.54827	–1.51314	–1.53814	–1.53812
1.0	–1.41902	–1.35862	–1.45199	–1.41346	–1.44388	–1.44292

Table 2
Poiseuille flow: velocity profile $u_p(y)$, $2a = 2$, $\alpha_t = 0.5$

y/a	BGK-CL $\alpha_n = 0.5$	BGK-CL $\alpha_n = 0.01$	BGK-DE [13] $\alpha = \alpha_t$
0.0	–3.647834	–3.653676	–3.652222
0.1	–3.640383	–3.646286	–3.644836
0.2	–3.617928	–3.624011	–3.622577
0.3	–3.580145	–3.586524	–3.585117
0.4	–3.526441	–3.533223	–3.531852
0.5	–3.455844	–3.463117	–3.461789
0.6	–3.366792	–3.374602	–3.373321
0.7	–3.256671	–3.264970	–3.263728
0.8	–3.120647	–3.129168	–3.127917
0.9	–2.947672	–2.955481	–2.954020
1.0	–2.678901	–2.680443	–2.676407

Table 3
Poiseuille flow: the flow rate U_p, $\alpha_t = 0.5$

$2a$	S-CL [26] $\alpha_n = 0.5$	S-DE [26] $\alpha = \alpha_t$	BGK-CL $\alpha_n = 0.5$	BGK-CL $\alpha_n = 0.01$	BGK-DE [13] $\alpha = \alpha_t$
0.01	–5.014219	–7.210007	–5.011569	–6.491368	–
0.02	–4.668298	–6.298270	–4.664196	–5.909004	–
0.03	–4.474712	–5.808061	–4.469520	–5.550575	–
0.04	–4.342079	–5.482139	–4.335982	–5.293481	–
0.05	–4.242237	–5.242765	–4.235359	–5.095217	–5.223297
0.07	–4.097278	–4.905303	–4.089094	–4.802865	–
0.09	–3.993879	–4.672567	–3.984625	–4.593247	–
0.1	–3.951889	–4.580089	–3.942165	–4.508329	–4.556407
0.3	–3.573656	–3.806140	–3.558721	–3.770488	–3.778472
0.5	–3.447263	–3.571767	–3.430280	–3.541575	–3.544371
0.7	–3.388287	–3.464010	–3.370373	–3.436681	–3.437669
0.9	–3.359841	–3.409028	–3.341530	–3.383783	–3.383887
1.0	–3.352483	–3.392769	–3.334088	–3.368405	–3.368218
3.0	–3.499791	–3.503677	–3.483401	–3.488489	–
3.5	–3.565466	–3.569734	–3.549687	–3.555699	–
4.0	–3.634859	–3.640058	–3.619647	–3.626974	–
5.0	–3.780735	–3.788425	–3.766531	–3.776820	–3.774402
6.0	–3.932453	–3.942771	–3.919108	–3.932276	–
7.0	–4.087720	–4.100498	–4.075113	–4.090881	–4.088108
9.0	–4.404578	–4.421533	–4.393176	–4.413231	–4.410190
10.0	–4.565036	–4.583722	–4.554131	–4.575935	–
100.0	–19.50102	–19.53951	–19.49650	–19.53765	–

Table 4
Poiseuille flow: heat-flow profile $q_p(y)$, $2a = 1$, $\alpha_t = 0.5$

y/a	S-CL [26] $\alpha_n = 0.5$	S-DE [26] $\alpha = \alpha_t$	BGK-CL $\alpha_n = 0.5$	BGK-CL $\alpha_n = 0.01$	BGK-DE [30] $\alpha = \alpha_t$
0.0	2.40629(–1)	2.76699(–1)	1.91854(–1)	2.09741(–1)	2.10798(–1)
0.1	2.39761(–1)	2.75924(–1)	1.91160(–1)	2.09107(–1)	2.10167(–1)
0.2	2.37134(–1)	2.73578(–1)	1.89055(–1)	2.07185(–1)	2.08251(–1)
0.3	2.32674(–1)	2.69595(–1)	1.85470(–1)	2.03911(–1)	2.04989(–1)
0.4	2.26248(–1)	2.63856(–1)	1.80281(–1)	1.99171(–1)	2.00264(–1)
0.5	2.17640(–1)	2.56164(–1)	1.73281(–1)	1.92774(–1)	1.93887(–1)
0.6	2.06511(–1)	2.46210(–1)	1.64148(–1)	1.84423(–1)	1.85559(–1)
0.7	1.92299(–1)	2.33480(–1)	1.52348(–1)	1.73622(–1)	1.74779(–1)
0.8	1.73992(–1)	2.17035(–1)	1.36911(–1)	1.59466(–1)	1.60635(–1)
0.9	1.49341(–1)	1.94755(–1)	1.15681(–1)	1.39934(–1)	1.41067(–1)
1.0	1.06894(–1)	1.55516(–1)	7.77162(–2)	1.04677(–1)	1.05346(–1)

Table 5
Poiseuille flow: the heat-flow rate Q_p, $\alpha_t = 0.5$

$2a$	S-CL [26] $\alpha_n = 0.5$	S-DE [26] $\alpha = \alpha_t$	BGK-CL $\alpha_n = 0.5$	BGK-CL $\alpha_n = 0.01$	BGK-DE [30] $\alpha = \alpha_t$
0.01	1.423000	2.770617	1.408981	2.352043	–
0.02	1.249702	2.311215	1.228046	2.038897	–
0.03	1.151878	2.060542	1.124381	1.841613	–
0.04	1.084182	1.891307	1.051862	1.697491	–
0.05	1.032667	1.765080	9.962174(–1)	1.584570	–
0.07	9.566156(–1)	1.583132	9.133327(–1)	1.414610	–
0.09	9.010436(–1)	1.453788	8.522460(–1)	1.289586	–
0.1	8.780440(–1)	1.401214	8.268522(–1)	1.238012	1.2664
0.3	6.471470(–1)	9.094469(–1)	5.712674(–1)	7.507963(–1)	–
0.5	5.444746(–1)	7.155058(–1)	4.607790(–1)	5.663927(–1)	–
0.7	4.786409(–1)	6.004731(–1)	3.926452(–1)	4.619360(–1)	–
0.9	4.307185(–1)	5.216112(–1)	3.448332(–1)	3.929745(–1)	–
1.0	4.110242(–1)	4.904286(–1)	3.256784(–1)	3.663468(–1)	3.6854(–1)
3.0	2.272407(–1)	2.349312(–1)	1.627443(–1)	1.629235(–1)	–
3.5	2.056379(–1)	2.091089(–1)	1.455576(–1)	1.438762(–1)	–
4.0	1.879290(–1)	1.885784(–1)	1.317739(–1)	1.289338(–1)	–
5.0	1.604938(–1)	1.578737(–1)	1.109510(–1)	1.069215(–1)	–
6.0	1.401296(–1)	1.359157(–1)	9.589976(–2)	9.142776(–2)	–
7.0	1.243653(–1)	1.193805(–1)	8.447597(–2)	7.989805(–2)	–
9.0	1.014953(–1)	9.606501(–2)	6.823850(–2)	6.384237(–2)	–
10.0	9.292892(–2)	8.752351(–2)	6.225335(–2)	5.801937(–2)	5.8364(–2)
100.0	1.065782(–2)	9.670226(–3)	6.945731(–3)	6.283500(–3)	–

6. Computational aspects and numerical results

To evaluate Eqs. (70) to (82), the first step is to define the quadrature scheme associated to the ADO method. In this sense, for most of the problems in the rarefied gas dynamics field, that have been solved by this method [13,17,19], the following approach has been shown to be adequate for several cases, which is: to map the interval of integration into the interval $[0, 1]$ and then map the Gauss–Legendre points linearly to this interval. In general, the expression

$$u(\xi) = \mathrm{e}^{-\xi} \tag{83}$$

is the one used to map the interval $[0, \infty)$ into $[0, 1]$.

Once the quadrature scheme is defined, the next steps are: to get the eigenvalues (separation constants) by solving Eq. (47) with a numerical linear algebra routine available; to evaluate Eqs. (51) to obtain the numerical elementary solutions; to solve the linear system defined either by Eq. (57) or (62) and then the expressions needed, Eqs. (66) to (82), for obtaining the quantities of interest. We used $N = 60$ to generate the results shown in Tables 1 to 16. In addition, in order to compare with results available

Table 6
Thermal creep flow: velocity profile $u_t(y)$, $2a = 1$, $\alpha_t = 0.5$

y/a	S-CL [26] $\alpha_n = 0.5$	S-CL ($\varepsilon = \varepsilon_t$) $\alpha_n = 0.5$	S-DE [26] $\alpha = \alpha_t$	S-DE ($\varepsilon = \varepsilon_t$) $\alpha = \alpha_t$	BGK-CL $\alpha_n = 0.5$	BGK-CL $\alpha_n = 0.01$	BGK-DE [30] $\alpha = \alpha_t$
0.0	2.308391(–1)	1.919736(–1)	2.637228(–1)	2.072228(–1)	1.817431(–1)	1.964317(–1)	1.97421(–1)
0.1	2.302050(–1)	1.914082(–1)	2.632585(–1)	2.068150(–1)	1.812832(–1)	1.961068(–1)	1.97099(–1)
0.2	2.282867(–1)	1.896966(–1)	2.618543(–1)	2.055803(–1)	1.798898(–1)	1.951227(–1)	1.96124(–1)
0.3	2.250342(–1)	1.867894(–1)	2.594743(–1)	2.034830(–1)	1.775206(–1)	1.934508(–1)	1.94467(–1)
0.4	2.203564(–1)	1.825971(–1)	2.560532(–1)	2.004582(–1)	1.740981(–1)	1.910384(–1)	1.92076(–1)
0.5	2.141065(–1)	1.769753(–1)	2.514854(–1)	1.964009(–1)	1.694970(–1)	1.878008(–1)	1.88867(–1)
0.6	2.060530(–1)	1.696965(–1)	2.456037(–1)	1.911447(–1)	1.635198(–1)	1.836038(–1)	1.84707(–1)
0.7	1.958173(–1)	1.603891(–1)	2.381337(–1)	1.844162(–1)	1.558426(–1)	1.782275(–1)	1.79377(–1)
0.8	1.827199(–1)	1.483853(–1)	2.285787(–1)	1.757189(–1)	1.458836(–1)	1.712760(–1)	1.72482(–1)
0.9	1.652605(–1)	1.322075(–1)	2.158304(–1)	1.639392(–1)	1.323593(–1)	1.618736(–1)	1.63143(–1)
1.0	1.358984(–1)	1.043407(–1)	1.941861(–1)	1.432429(–1)	1.088709(–1)	1.456356(–1)	1.46896(–1)

Table 7
Thermal creep flow: velocity profile $u_t(y)$, $2a = 2$, $\alpha_t = 0.5$

y/a	BGK-CL $\alpha_n = 0.5$	BGK-CL $\alpha_n = 0.01$	BGK-DE [13] $\alpha = \alpha_t$
0.0	2.426222(–1)	2.427729(–1)	2.439084(–1)
0.1	2.419790(–1)	2.423235(–1)	2.434617(–1)
0.2	2.400252(–1)	2.409587(–1)	2.421049(–1)
0.3	2.366844(–1)	2.386258(–1)	2.397858(–1)
0.4	2.318170(–1)	2.352282(–1)	2.364086(–1)
0.5	2.251967(–1)	2.306091(–1)	2.318176(–1)
0.6	2.164632(–1)	2.245185(–1)	2.257644(–1)
0.7	2.050225(–1)	2.165425(–1)	2.178377(–1)
0.8	1.897959(–1)	2.059261(–1)	2.072854(–1)
0.9	1.683751(–1)	1.909713(–1)	1.924101(–1)
1.0	1.284482(–1)	1.628985(–1)	1.643019(–1)

Table 8
Thermal creep flow: heat-flow profile $q_t(y)$, $2a = 1$, $\alpha_t = 0.5$

y/a	S-CL [26] $\alpha_n = 0.5$	S-CL ($\varepsilon = \varepsilon_t$) $\alpha_n = 0.5$	S-DE [26] $\alpha = \alpha_t$	S-DE ($\varepsilon = \varepsilon_t$) $\alpha = \alpha_t$	BGK-CL $\alpha_n = 0.5$	BGK-CL $\alpha_n = 0.01$
0.0	–1.054961	–8.406252(–1)	–1.288279	–9.699612(–1)	–8.324107(–1)	–8.581441(–1)
0.1	–1.052822	–8.388598(–1)	–1.286901	–9.688383(–1)	–8.308898(–1)	–8.567083(–1)
0.2	–1.046342	–8.335008(–1)	–1.282727	–9.654309(–1)	–8.262728(–1)	–8.523496(–1)
0.3	–1.035317	–8.243511(–1)	–1.275633	–9.596181(–1)	–8.183888(–1)	–8.449075(–1)
0.4	–1.019378	–8.110515(–1)	–1.265393	–9.511789(–1)	–8.069264(–1)	–8.340890(–1)
0.5	–9.979281(–1)	–7.930222(–1)	–1.251644	–9.397570(–1)	–7.913820(–1)	–8.194206(–1)
0.6	–9.700305(–1)	–7.693464(–1)	–1.233812	–9.247884(–1)	–7.709593(–1)	–8.001538(–1)
0.7	–9.341567(–1)	–7.385250(–1)	–1.210963	–9.053494(–1)	–7.443553(–1)	–7.750640(–1)
0.8	–8.875782(–1)	–6.978693(–1)	–1.181426	–8.797795(–1)	–7.092343(–1)	–7.419569(–1)
0.9	–8.243358(–1)	–6.414761(–1)	–1.141540	–8.444161(–1)	–6.604821(–1)	–6.960297(–1)
1.0	–7.153601(–1)	–5.403023(–1)	–1.073270	–7.810084(–1)	–5.732521(–1)	–6.139726(–1)

in the literature, we used $k_1 = 1$, in defining the Poiseuille flow problem, $k_2 = 1$ for the thermal-creep problem and $k_3 = -u_w/a$ for the Couette flow problem ($\pm u_w$ are the velocities of the plate at $y = \mp a$).

In this work, in Tables 1 to 16, we present results for different cases, in the sense of using a wide range of the accommodation coefficients, including special cases ($\alpha_n \to 0$) where, according to the literature [26], the expected results should be similar to the specular case of the Maxwell boundary conditions. In fact, that was one way we used to check our program and have confidence in our results.

Table 9
Thermal creep flow: heat-flow profile $q_t(y)$, $2a = 1$, $\alpha_t = 0.1$

y/a	BGK-DE [30] $\alpha = \alpha_t$	BGK-CL $\alpha_n = 0.5$	BGK-CL $\alpha_n = 0.01$
0.0	–1.17929	–1.04123	–1.11177
0.1	–1.17908	–1.04057	–1.11129
0.2	–1.17847	–1.03857	–1.10986
0.3	–1.17743	–1.03516	–1.10743
0.4	–1.17592	–1.03020	–1.10389
0.5	–1.17388	–1.02350	–1.09911
0.6	–1.17121	–1.01472	–1.09285
0.7	–1.16778	–1.00332	–1.08474
0.8	–1.16329	–9.88329(–1)	–1.07412
0.9	–1.15715	–9.67637(–1)	–1.05951
1.0	–1.14642	–9.30924(–1)	–1.03384

Table 10
Couette flow: velocity profile $u_c(y)$, $u_w = 1$, $2a = 1$, $\alpha_t = 0.5$

y/a	BGK-CL $\alpha_n = 0.5$	BGK-CL $\alpha_n = 0.01$	S-CL $\alpha_n = 0.5$	S-DE [19] $\alpha = \alpha_t$
0.0	0.00	0.00	0.00	0.00
0.1	–2.082788(–2)	–2.180447(–2)	–2.093477(–2)	–2.19712(–2)
0.2	–4.173979(–2)	–4.372158(–2)	–4.195212(–2)	–4.40546(–2)
0.3	–6.282658(–2)	–6.587207(–2)	–6.314130(–2)	–6.63718(–2)
0.4	–8.419431(–2)	–8.839885(–2)	–8.460648(–2)	–8.90658(–2)
0.5	–1.059769(–1)	–1.114833(–1)	–1.064793(–1)	–1.12319(–1)
0.6	–1.283585(–1)	–1.353764(–1)	–1.289403(–1)	–1.36383(–1)
0.7	–1.516183(–1)	–1.604616(–1)	–1.522640(–1)	–1.61646(–1)
0.8	–1.762423(–1)	–1.874103(–1)	–1.769277(–1)	–1.88791(–1)
0.9	–2.033003(–1)	–2.177064(–1)	–2.039830(–1)	–2.19337(–1)
1.0	–2.383022(–1)	–2.589842(–1)	–2.388559(–1)	–2.61279(–1)

Table 11
Couette flow: velocity profile $u_c(y)$, $u_w = 1$, $2a = 1$, $\alpha_t = 1.0$

y/a	BGK-DE $\alpha = \alpha_t$	BGK-CL $\alpha_n = 0.5$	S-DE $\alpha = \alpha_t$	S-CL $\alpha_n = 0.5$
0.0	0.00	0.00	0.00	0.00
0.1	–4.444980(–2)	–4.444980(–2)	–4.464054(–2)	–4.464054(–2)
0.2	–8.906388(–2)	–8.906388(–2)	–8.944244(–2)	–8.944244(–2)
0.3	–1.340199(–1)	–1.340199(–1)	–1.345802(–1)	–1.345802(–1)
0.4	–1.795258(–1)	–1.795258(–1)	–1.802581(–1)	–1.802581(–1)
0.5	–2.258445(–1)	–2.258445(–1)	–2.267341(–1)	–2.267341(–1)
0.6	–2.733383(–1)	–2.733383(–1)	–2.743641(–1)	–2.743641(–1)
0.7	–3.225586(–1)	–3.225586(–1)	–3.236894(–1)	–3.236894(–1)
0.8	–3.744672(–1)	–3.744672(–1)	–3.756547(–1)	–3.756547(–1)
0.9	–4.311896(–1)	–4.311896(–1)	–4.323489(–1)	–4.323489(–1)
1.0	–5.037226(–1)	–5.037226(–1)	–5.045992(–1)	–5.045992(–1)

We present in tables, in addition to the "BGK-CL" results (BGK model with Cercignani–Lampis boundary conditions) obtained with the formulation presented in this work, the "S-CL" results (S model with Cercignani–Lampis boundary conditions) we obtained [31] by including the Cercignani–Lampis boundary conditions to the formulation developed by Cabrera and Barichello [19], in which, in contrast to Ref. [26], the parameter ε was considered arbitrary. In fact, for the S-model, Eq. (4) assumes different values when evaluated in terms of viscosity ($\varepsilon_p = 1$) or thermal conductivity ($\varepsilon_t = 3/2$) [19]. In generating some of the results presented in the tables, we used, in general, $\varepsilon = \varepsilon_p$. We still note that, we also use the notation "DE" to reference results associated to the diffuse-specular boundary conditions.

Table 12
Couette flow: heat-flow profile $q_c(y)$, $u_w = 1$, $2a = 1$, $\alpha_t = 0.5$

y/a	BGK-CL $\alpha_n = 0.5$	BGK-CL $\alpha_n = 0.01$	S-CL $\alpha_n = 0.5$	S-DE [19] $\alpha = \alpha_t$
0.0	0.00	0.00	0.00	0.00
0.1	2.747698(–3)	3.290843(–3)	3.172930(–3)	3.86036(–3)
0.2	5.537417(–3)	6.637746(–3)	6.383073(–3)	7.77360(–3)
0.3	8.414572(–3)	1.010147(–2)	9.670515(–3)	1.17969(–2)
0.4	1.143220(–2)	1.375334(–2)	1.308180(–2)	1.59974(–2)
0.5	1.465727(–2)	1.768404(–2)	1.667532(–2)	2.04597(–2)
0.6	1.818182(–2)	2.201906(–2)	2.053075(–2)	2.53011(–2)
0.7	2.214549(–2)	2.695015(–2)	2.476839(–2)	3.07006(–2)
0.8	2.679122(–2)	3.281295(–2)	2.959705(–2)	3.69732(–2)
0.9	3.265398(–2)	4.034949(–2)	3.547748(–2)	4.48226(–2)
1.0	4.248871(–2)	5.337687(–2)	4.481701(–2)	5.80004(–2)

Table 13
Couette flow: heat-flow profile $q_c(y)$, $u_w = 1$, $2a = 1$, $\alpha_t = 1.0$

y/a	S-DE $\alpha = \alpha_t$	S-CL $\alpha_n = 0.5$	BGK-DE $\alpha = \alpha_t$	BGK-CL $\alpha_n = 0.5$
0.0	0.00	0.00	0.00	0.00
0.1	6.075741(–3)	6.075741(–3)	5.278643(–3)	5.278643(–3)
0.2	1.222416(–2)	1.222416(–2)	1.063943(–2)	1.063943(–2)
0.3	1.852364(–2)	1.852364(–2)	1.617119(–2)	1.617119(–2)
0.4	2.506532(–2)	2.506532(–2)	2.197786(–2)	2.197786(–2)
0.5	3.196381(–2)	3.196381(–2)	2.819096(–2)	2.819096(–2)
0.6	3.937594(–2)	3.937594(–2)	3.499163(–2)	3.499163(–2)
0.7	4.753920(–2)	4.753920(–2)	4.265551(–2)	4.265551(–2)
0.8	5.686717(–2)	5.686717(–2)	5.166358(–2)	5.166358(–2)
0.9	6.827561(–2)	6.827561(–2)	6.307849(–2)	6.307849(–2)
1.0	8.657217(–2)	8.657217(–2)	8.239876(–2)	8.239876(–2)

Table 14
Couette flow: the flow rate U_c, $u_w = 1$, $\alpha_t = 0.5$

$2a$	BGK-CL $\alpha_n = 0.01$	BGK-DE [16] $\alpha = \alpha_t$	S-CL $\alpha_n = 0.5$	S-DE [32] $\alpha = \alpha_t$	BGK-CL $\alpha_n = 0.5$
1.0(–1)	–2.643973(–1)	–2.74926(–1)	–2.447809(–1)	–2.75239(–1)	–2.445556(–1)
1.0	–1.056692(–1)	–1.16120(–1)	–1.096461(–1)	–1.16739(–1)	–1.092005(–1)
1.0(1)	–2.764398(–2)	–3.26636(–2)	–3.270622(–2)	–3.27074(–2)	–3.267069(–2)

Table 15
Couette flow: the heat-flow rate Q_c, $u_w = 1$, $\alpha_t = 0.5$

$2a$	BGK-CL $\alpha_n = 0.01$	BGK-DE [16] $\alpha = \alpha_t$	S-CL $\alpha_n = 0.5$	S-DE [32] $\alpha = \alpha_t$	BGK-CL $\alpha_n = 0.5$
1.0(–1)	9.980679(–2)	9.17172(–2)	7.750149(–2)	9.31118(–2)	7.649576(–2)
1.0	2.610433(–2)	1.99715(–2)	1.809911(–2)	2.25189(–2)	1.626907(–2)
1.0(1)	9.127214(–4)	4.29861(–4)	4.890106(–4)	6.09261(–4)	3.537455(–4)

To have some confidence in our results, which we believe to be correct for all the digits presented in the tables (plus or minus one in the last digit), we established comparisons with results available in the literature for other models [7,26] and we found good agreement. We also use the special cases to establish comparisons with the diffuse-specular results. As it has been found for other problems [19,32] the results based on the BGK and S model, have, in general, agreement in one or two digits, for an adequate choice of the mean-free-path.

Table 16
Couette flow: a component P_{xy} of the pressure tensor, $u_w = 1$, $\alpha_t = 1.0$

$2a$	BGK-CL $\alpha_n = 0.01$	BGK-DE $\alpha = \alpha_t$	S-CL $\alpha_n = 0.5$	S-DE $\alpha = \alpha_t$	BGK-CL $\alpha_n = 0.5$
1.0(–2)	9.913980(–1)	9.913980(–1)	9.913980(–1)	9.913980(–1)	9.913980(–1)
2.0(–2)	9.831755(–1)	9.831755(–1)	9.811753(–1)	9.811753(–1)	9.831755(–1)
1.0(–1)	9.257968(–1)	9.257968(–1)	9.257894(–1)	9.257894(–1)	9.257968(–1)
1.0	6.007292(–1)	6.007292(–1)	6.005436(–1)	6.005436(–1)	6.007292(–1)
2.0	4.436467(–1)	4.436467(–1)	4.434197(–1)	4.434197(–1)	4.436467(–1)
3.0	3.535337(–1)	3.535337(–1)	3.533315(–1)	3.533315(–1)	3.535337(–1)
1.0(1)	1.473125(–1)	1.473125(–1)	1.472598(–1)	1.472598(–1)	1.473125(–1)
2.0(1)	8.044769(–2)	8.044769(–2)	8.043177(–2)	8.043177(–2)	8.044769(–2)
1.0(3)	1.768859(–3)	1.768859(–3)	1.768851(–2)	1.768851(–2)	1.768859(–3)
1.0(7)	1.772453(–7)	1.772453(–7)	1.772453(–7)	1.772453(–7)	1.772453(–7)

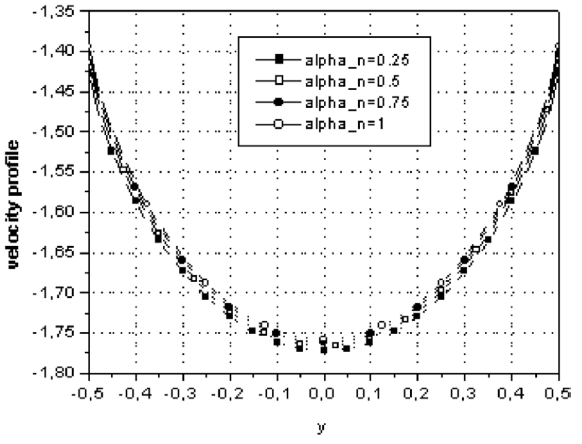

Fig. 1. Poiseuille flow – BGK model – velocity profile, $2a = 1$ and $\alpha_t = 0.5$.

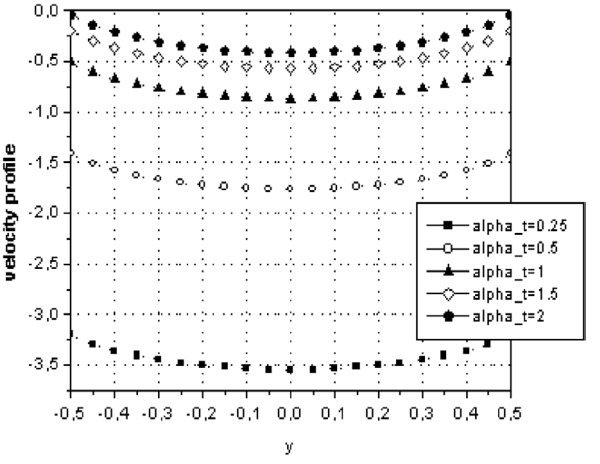

Fig. 2. Poiseuille flow – BGK model – velocity profile, $2a = 1$ and $\alpha_n = 0.5$.

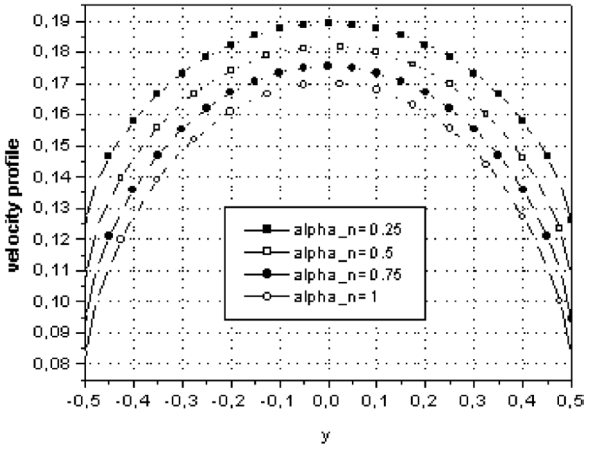

Fig. 3. Thermal-creep flow – BGK model – velocity profile, $2a = 1$ and $\alpha_t = 0.5$.

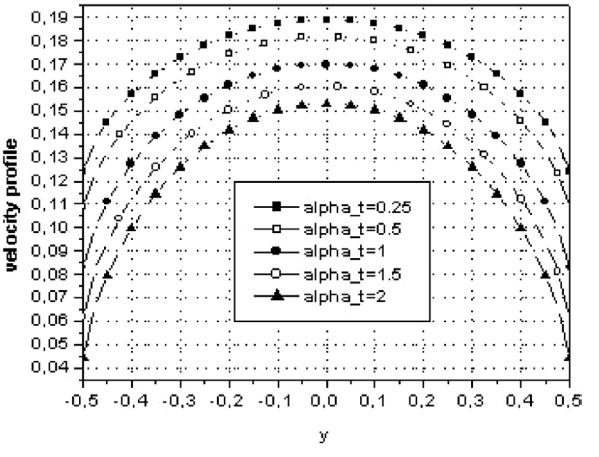

Fig. 4. Thermal-creep flow – BGK model – velocity profile, $2a = 1$ and $\alpha_n = 0.5$.

We also reproduce some graphs (Figs. 1 to 6) to emphasize that the results, that do not seem to be sensitive to the model, are very sensitive to the accommodation coefficients, mainly, the tangential accommodation coefficient.

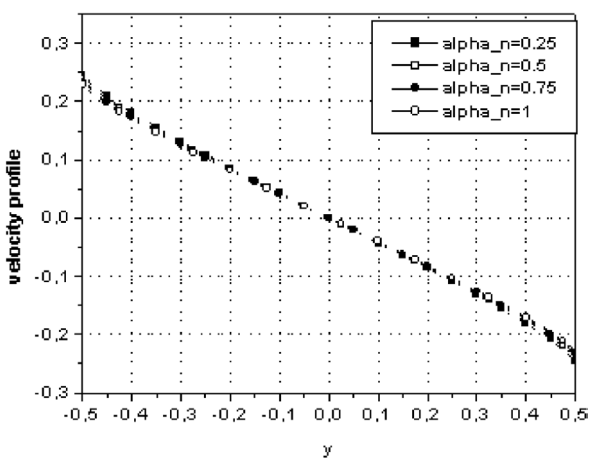

Fig. 5. Couette flow – BGK model – velocity profile, $2a = 1$ and $\alpha_t = 0.5$.

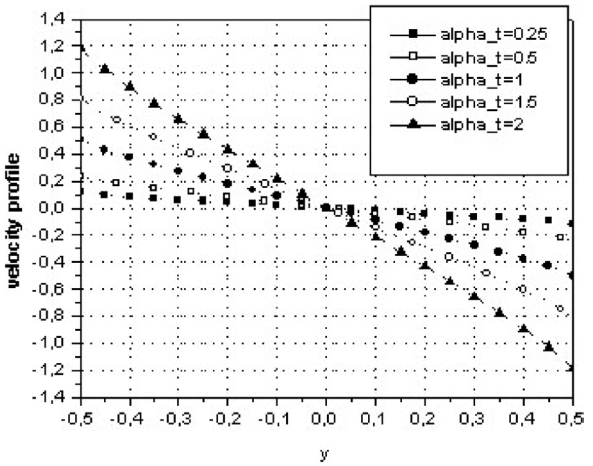

Fig. 6. Couette flow – BGK model – velocity profile, $2a = 1$ and $\alpha_n = 0.5$.

7. Concluding comments

The ADO method, an analytical version of the discrete-ordinates method, based on a half-range quadrature scheme, was used to develop in an unified way, a solution for the Poiseuille, thermal-creep and Couette flow problems, in the rarefied dynamics field, with the gas–surface interaction modeled by the Cercignani–Lampis kernel. The results based on the BGK model do not show a significant difference in comparison with other constant collision frequency model (S-model) treated by the same approach, but it was noted, on the other hand, the dependence on the accommodation coefficients variation, in particular, the tangential accommodation coefficient.

Acknowledgements

The authors would like to thank F. Sharipov for helpful discussions regarding to this work and to CAPES and CNPq of Brasil for financial support.

References

[1] G.E. Karniadakis, A. Beskok, Micro Flows, Springer-Verlag, New York, 2002.
[2] C. Cercignani, Rarefied Gas Dynamics From Basic Concepts to Actual Calculations, Cambridge University Press, Cambridge, 2000.
[3] M.M.R. Williams, A review of the rarefied gas dynamics theory associated with some classical problems in flow and heat transfer, Z. Angew. Math. Phys. 52 (2001) 500.
[4] T. Klinc, I. Kuščer, Slip coefficients for general gas–surface interaction, Phys. Fluids 15 (1972) 1018.
[5] R. Lord, Some extensions of the Cercignani–Lampis gas–surface scattering kernel, Phys. Fluids A 3 (1991) 706.
[6] C. Cercignani, M. Lampis, Kinetic models for gas–surface interaction, Transport Theory Statist. Phys. 1 (1971) 101.
[7] F. Sharipov, Application of the Cercignani–Lampis scattering kernel to calculations of rarefied gas flows. I. Plane flow between two parallel plates, Eur. J. Mech. B/Fluids 21 (2002) 113.
[8] F. Sharipov, Application of the Cercignani–Lampis scattering kernel to calculations of rarefied gas flows. II. Slip and jump coefficients, Eur. J. Mech. B/Fluids 22 (2003) 133.
[9] F. Sharipov, Application of the Cercignani–Lampis scattering kernel to calculations of rarefied gas flows. III. Poiseuille flow and thermal creep through a long tube, Eur. J. Mech. B/Fluids 22 (2003) 145.
[10] C. Cercignani, M. Lampis, S. Lorenzani, Plane Poiseuille flow with symmetric and nonsymmetric gas–wall interactions, Transport Theory Statist. Physics (2004), in press.
[11] L.B. Barichello, C.E. Siewert, A discrete-ordinates solution for a non-grey model with complete frequency redistribution, JQSRT 62 (1999) 665.
[12] L.B. Barichello, C.E. Siewert, A discrete-ordinates solution for Poiseuille flow in a plane channel, Z. Angew. Math. Phys. 50 (1999) 972.
[13] L.B. Barichello, M. Camargo, P. Rodrigues, C.E. Siewert, Unified solutions to classical flow problems based on the BGK model, Z. Angew. Math. Phys. 52 (2001) 1.

[14] L.B. Barichello, C.E. Siewert, The temperature-jump problem in rarefied gas dynamics, Eur. J. Appl. Math. 11 (2000) 353.
[15] L.B. Barichello, A.C.R. Bartz, M. Camargo, C.E. Siewert, The temperature-jump problem for a variable collision frequency model, Phys. Fluids 14 (2002) 382.
[16] C.E. Siewert, Poiseuille, thermal creep and Couette flow: results based on the CES model of the linearized Boltzmann equation, Eur. J. Mech. B/Fluids 21 (2002) 579.
[17] M. Camargo, L.B. Barichello, Unified approach for variable collision frequency models in rarefied gas dynamics, TTSP 33 (2004) 227.
[18] C.E. Siewert, The linearized Boltzmann equation: concise and accurate solutions to basic flow problems, Z. Angew. Math. Phys. 54 (2003) 273.
[19] L.C. Cabrera, L.B. Barichello, Unified solutions to some classical problems in rarefied gas dynamics based on the one-dimensional linearized S-model equations, Z. Angew. Math. Phys., in press.
[20] P.L. Bhatnagar, E.P. Gross, M. Krook, A model for collision processes in gases. I. Small amplitude processes in charged and neutral one-component systems, Phys. Rev. 94 (1954) 511.
[21] F. Sharipov, V. Seleznev, Data on internal rarefied gas flows, J. Phys. Chem. Ref. Data 27 (1998) 657.
[22] C. Cercignani, The method of elementary solutions for kinetic models with velocity-dependent collision frequency, Ann. Phys. (NY) 40 (1966) 469.
[23] S.K. Loyalka, J.H. Ferziger, Model dependence of the temperature slip coefficient, Phys. Fluids 11 (1968) 1668.
[24] L.B. Barichello, C.E. Siewert, Some comments on modeling the linearized Boltzmann equation, JQSRT 77 (2003) 43.
[25] C. Cercignani, The Boltzmann Equation and Its Applications, Springer-Verlag, New York, 1988.
[26] C.E. Siewert, Generalized boundary conditions for the S-model kinetic equations basic to flow in a plane channel, JQSRT 72 (2002) 75.
[27] C.E. Siewert, F. Sharipov, Model equations in rarefied gas dynamics: viscous-slip and thermal-slip coefficients, Phys. Fluids 14 (2002) 4123.
[28] R.F. Knackfuss, L.B. Barichello, A discrete-ordinates solution to the Poiseuille flow problem in the rarefied gas dynamics based on the BGK model with generalized boundary conditions, in: Iberian American Congress on Computational Methods in Engineering – CILAMCE 2003, Ouro Preto, MG, Brasil, 2003.
[29] C.E. Siewert, Viscous-slip, thermal-slip and temperature-jump coefficients as defined by linearized Boltzmann equation and the Cercignani–Lampis boundary condition, Phys. Fluids 15 (2003) 1696.
[30] M. Camargo, Unified solutions for variable collision frequency models in rarefied gas dynamics, PhD Thesis, Graduate Program in Mechanical Engineering, Universidade Federal do Rio Grande do Sul, Porto Alegre, RS, Brasil, 2003 (in Portuguese).
[31] R.F. Knackfuss, L.B. Barichello, Rarefied gas dynamics in microchannels, in: Brazilian Congress in Computational and Applied Mathematics, Porto Alegre, RS, Brasil, 2004 (in Portuguese).
[32] L.C. Cabrera, Derivation and solution of model equations in the rarefied gas dynamics, MsC Dissertation, Graduate Program in Applied Mathematics, Porto Alegre, RS, Brasil, 2003 (in Portuguese).